Transport in Porous Media (2005) 61:215–233
DOI 10.1007/s11242-004-7906-6

Extensions to the Macroscopic Navier–Stokes Equation

S. SOREK[1,2], D. LEVI-HEVRONI[2], A. LEVY[2] and G. BEN-DOR[2]
[1]*Department of Environmental Hydrology & Microbiology, Sde Boker Campus, Institute for Water Sciences and Technologies, Blaustein Institutes for Desert Reasearch, Ben-Gurion University of the Negev, Israel*
[2]*Department of Mechanical Engineering, Pearlstone Center for Aeronautical Engineering Studies, Beer-Sheva, Israel*

(Received: 9 June 2004; accepted in final form: 16 December 2004)

Abstract. A development is provided showing that for any phase, by not neglecting the macroscopic terms of the deviation from the intensive momentum and of the dispersive momentum, we obtain a macroscopic secondary momentum balance equation coupled with a macroscopic dominant momentum balance equation that is valid at a larger spatial scale. The macroscopic secondary momentum balance equation is in the form of a wave equation that propagates the deviation from the intensive momentum while concurrently, in the case of a Newtonian fluid and under certain assumptions, the macroscopic dominant momentum balance equation may be approximated by Darcy's equation to address drag dominant flow. We then develop extensions to the dominant macroscopic Navier–Stokes (*NS*) equation for saturated porous matrices, to account for the pressure gradient at the microscopic solid-fluid interfaces. At the microscopic interfaces we introduce the exchange of inertia between the phases, accounting for the relative fluid square velocities and the rate of these velocities, interpreted as Forchheimer terms. Conditions are provided to approximate the extended dominant *NS* equation by Forchheimer quadratic momentum law or by Darcy's linear momentum law. We also show that the dominant *NS* equation can conform into a nonlinear wave equation. The one-dimensional numerical solution of this nonlinear wave equation demonstrates good qualitative agreement with experiments for the case of a highly deformable elasto-plastic matrix.

Key words: representative elementary volume, macroscopic momentum balance equation, spatial scaling, solid-fluid microscopic interface, saturated porous media, nonlinear wave propagation.

1. Introduction

Applying averaging rules to a *Representative Elementary Volume (REV)*, Bear and Bachmat (1990) formulated the macroscopic balance equations for interacting phases of fluids and a deformable porous matrix. Based on these, Bear and Sorek (1990) developed the dominant macroscopic forms of mass and momentum balance equations following an abrupt pressure impact in saturated porous materials under isothermal conditions. It was shown that during a certain time period, due to the domination of inertial terms, the fluid momentum balance equation conforms to a nonlinear wave equation. Bear *et al.* (1992) and Sorek *et al.* (1992), elaborated on these for the case of thermoelastic porous media, describing the theoretical basis for obtaining displacement and shock waves, respectively.

These models, however, excluded the possibility of the exchange of microscopic inertia through the solid–fluid interface. Following Sorek *et al.* (1992) and Levy *et al.* (1995) introduced additional Forchheimer terms and obtained a variety of nonlinear wave equation forms. These together with the development of the evolving balance equations following an abrupt simultaneous changes of the fluid temperature and pressure, are the major novel theoretical aspects with respect to Nikolaevskiy (1990).

A discussion about analytical and numerical developments of models to simulate wave propagation through porous medium, appears in Sorek *et al.* (1999). These modified models based on Sorek *et al.* (1992) and Levy *et al.* (1995), are compared to other existing models and to observations from shock tube experiments. The latter proved to yield very good agreement with numerical simulations of the model described by Levy *et al.* (1995), when considering rigid porous matrices.

A rigorous mathematical development accounting for the exchange of momentum and energy between phases at their common interfaces, appears in Levy *et al.* (1999). This, when referring to inertial terms associated with gradients of fluid velocity, formulate the expressions of Forchheimer terms at the solid–fluid and fluid–fluid interfaces.

Sorek *et al.* (1999) present the macroscopic fluid momentum balance equation, coupled with the dominant averaged one and built of flux terms deviating from the averaged terms.

In what follows we will present the detailed development of the macroscopic form of the extended Navier–Stokes (NS) equation. This will describe the secondary coupled momentum balance equation comprised of momentum fluxes deviating from the averaged ones. When addressing the averaged momentum equation, it will account for the microscopic exchange of momentum, at the solid–fluid interface, resulting also from the fluid velocity rate (i.e. extension to Forchheimer term). Finally, based on Levy *et al.* (1995) in reference to the macroscopic non linear wave equation, simulation will be provided for the propagation of a compaction wave through a one-dimensional highly deformable saturated porous medium.

2. The Macroscopic Momentum Balance Equation

The basic forms of the macroscopic balance equations for a phase, are presented by Bear and Bachmat (1990) for the case of a porous medium of general local geometry. These are based on volume averaging of the microscopic balance equations. Some of these averaging techniques will be key elements in obtaining our extensions of the macroscopic balance equations. These, e.g., are

$$\overline{e_{1\alpha}e_{2\alpha}}^{\alpha} = \overline{e_{1\alpha}}^{\alpha}\overline{e_{2\alpha}}^{\alpha} + \overline{\overset{\circ}{e}_{1\alpha}\overset{\circ}{e}_{2\alpha}}^{\alpha}, \quad \overline{e_{1\alpha} + e_{2\alpha}}^{\alpha} = \overline{e_{1\alpha}}^{\alpha} + \overline{e_{2\alpha}}^{\alpha}, \tag{2.1}$$

where $e_{1\alpha}$ and $e_{2\alpha}$ denote two intensive quantities of the α phase, $\overline{e_\alpha}^{\alpha}$ denotes the average of e_α, over $\mathcal{U}_{o\alpha}$ the volume of α within $\mathcal{U}_o$ the volume of the *REV* and $\overset{\circ}{e}_\alpha (= e_\alpha - \overline{e_\alpha}^{\alpha})$ denotes deviation from the average $(\overline{e_\alpha}^{\alpha})$ of the intensive quantity of the α phase.

Modified rule (Bear and Bachmat, 1990) for averaging a spatial derivative

$$\overline{\frac{\partial e}{\partial x_i}}^{\alpha} \cong \frac{\partial \overline{e}^{\alpha}}{\partial x_j} T^*_{\alpha ij} + \frac{1}{\theta_\alpha \mathcal{U}_o} \int_{S_{\alpha\beta}} \overset{\circ}{x}_i \frac{\partial_e}{\partial x_j} \xi_{\alpha j} \, \mathrm{d}S, \tag{2.2}$$

here $\overset{\circ}{x}_i$ denotes the i-th coordinate of a point on the $\alpha - \beta$ interface ($S_{\alpha\beta}$ denotes the surface of these interfaces) relative to the *REV* centroid, $\boldsymbol{\xi}_\alpha$ denotes the unit vector outward to the α phase and θ_α $(= \mathcal{U}_{o\alpha}/\mathcal{U}_o)$ denotes the volume ratio of this phase. Bear and Bachmat (1990), assumed that the modified rule can be justified for the fluid (f) pressure (P) when $\nabla^2 P = 0$ in $\mathcal{U}_{of}$, namely that P has not an extremum distribution. Moreover, for $e \equiv P$, the second term on the r.h.s. of (2.2) allows the exchange of ∇P (at $\mathcal{S}_{\alpha\beta}$) with other momentum flux terms of the microscopic *NS* equation. Instead of (2.2) the averaged gradient approximation, in Nikolaevskiy *et al.* (1970) , Nikolaevskiy (1990, 1996) we find the notion of mass-averaged $\widehat{e}(= \overline{\rho e}/\overline{\rho})$ variable, the deviation $\widetilde{e}(= e - \widehat{e})$ from the mass-averaged variable and that of a phase interaction force, leading to an inertia resistance term which is introduced in the macroscopic fluid momentum equation.

The tensorial tortuosity coefficient, $T^*_{\alpha ij}$, appearing in (2.2) is defined by

$$T^*_{\alpha ij} = \frac{1}{\theta_\alpha \mathcal{U}_o} \int_{S_{\alpha\alpha}} \overset{\circ}{x}_i \xi_{\alpha j} \, \mathrm{d}S, \tag{2.3}$$

where $S_{\alpha\alpha}$ denotes the $\alpha - \alpha$ part of the *REV* boundary. This macroscopic coefficient reflects the microscopic configuration of the solid–fluid interface.

2.1. THE SECONDARY MOMENTUM BALANCE EQUATION

Following Bear and Bachmat (1990), the macroscopic (i.e. averaged over the *REV*) momentum balance equation of a phase, reads

$$\frac{D_\vartheta}{Dt}\left(\theta_\alpha \overline{\rho_\alpha \mathbf{V}_\alpha^m}^\alpha\right) = -\nabla \cdot \left[\theta_\alpha (\overline{\rho_\alpha \mathbf{V}_\alpha^m \mathbf{V}_\alpha^m - \boldsymbol{\sigma}_\alpha}^\alpha)\right] + \theta_\alpha \overline{\rho_\alpha \mathbf{F}_\alpha}^\alpha - \\ -\frac{1}{\mathcal{U}_\circ} \int_{\mathcal{S}_{\alpha\beta}} [\rho_\alpha \mathbf{V}_\alpha^m (\mathbf{V}_\alpha^m - \boldsymbol{\vartheta}) - \boldsymbol{\sigma}_\alpha] \cdot \boldsymbol{\xi}_\alpha \, dS, \tag{2.4}$$

where $D\vartheta/Dt \equiv \partial/\partial t + \boldsymbol{\vartheta} \cdot \nabla$ denotes the *material derivative*, which expresses the rate of change from the point of view of an observer traveling at the velocity, $\boldsymbol{\vartheta}$ (in (2.4) this velocity refers to the deforming surface enclosing $\mathcal{U}_\circ$), ρ_α denotes the density of the α phase, $\mathbf{V}_\alpha^m$ denotes the mass weighted velocity of the α phase, $\mathbf{F}_\alpha$ denotes the body force acting on the α phase and $\boldsymbol{\sigma}_\alpha$ denotes its stress.

Let us assume that:

[A.1] The $\mathcal{S}_{\alpha\beta}$ surface is material to the momentum flux of the phases,
[A.2] Very large Strouhal number ($St^{(\overline{e_\alpha}, \vartheta_c)} \gg 1$),

where $St^{(\overline{e_\alpha}, \vartheta_c)} \left(\equiv (L_c^{\overline{e_\alpha}}/t_c^{\overline{e_\alpha}}) \big/ \vartheta_c\right)$ is associated with the characteristic length increment ($L_c^{\overline{e_\alpha}}$) of the REV averaged $\overline{e_\alpha}$ ($=\theta_\alpha \overline{e_\alpha}^\alpha$, θ_α - volume ratio of the α phase) quantity, its characteristic time step ($t_c^{\overline{e_\alpha}}$), and the characteristic velocity (ϑ_c) of the deforming surface enclosing the REV.

In view of (2.1), [A.1] and [A.2], we rewrite (2.4) in the form:

$$\frac{\partial}{\partial t}\left[\theta_\alpha \left(\overline{\rho_\alpha}^\alpha \overline{\mathbf{V}_\alpha^m}^\alpha + \overline{\mathbf{d}_\alpha^M}^\alpha\right)\right] = -\nabla \cdot \left\{\theta_\alpha \left[\left(\overline{\rho_\alpha}^\alpha \overline{\mathbf{V}_\alpha^m}^\alpha + \overline{\mathbf{d}_\alpha^M}^\alpha\right) \overline{\mathbf{V}_\alpha^m}^\alpha + \\ + \overline{(\rho_\alpha \overset{\circ}{\mathbf{V}}{}_\alpha^m) \overset{\circ}{\mathbf{V}}{}_\alpha^m}^\alpha - \overline{\boldsymbol{\sigma}_\alpha}^\alpha\right]\right\} + \theta_\alpha \overline{\rho_\alpha \mathbf{F}_\alpha}^\alpha, \tag{2.5}$$

in which $\overline{\mathbf{d}_\alpha^M}^\alpha$ ($\equiv \overline{\overset{\circ}{\rho}_\alpha \overset{\circ}{\mathbf{V}}{}_\alpha^m}^\alpha$) denotes the deviation from the macroscopic intensive momentum ($\overline{\rho_\alpha \mathbf{V}_\alpha^m}^\alpha$) of the α phase.

Let us add the assumptions,

$$[A.3] \ \left|\overline{\rho_\alpha}^\alpha \overline{\mathbf{V}_\alpha^m}^\alpha\right| \gg \left|\overline{\mathbf{d}_\alpha^M}^\alpha\right|, \ \text{and} \ \ [A.4] \ \left|\overline{\rho_\alpha}^\alpha \overline{\mathbf{V}_\alpha^m}^\alpha \overline{\mathbf{V}_\alpha^m}^\alpha\right| \gg \left|\overline{(\rho_\alpha \overset{\circ}{\mathbf{V}}{}_\alpha^{0m}) \overset{\circ}{\mathbf{V}}{}_\alpha^{0m}}^\alpha\right|.$$

Following Biot (1956), a compressible fluid will behave as incompressible for a porous medium saturated with perfect fluid, when considering the seepage law (i.e. microscopic velocity field is a linear function of the phases average velocity components). This first-order approximation referring to the fluid density being constant over the REV, was demonstrated by Auriat *et al.* (1990) for a slow flow regime using an asymptotic method. Hence, for the fluid phase under such conditions, we can express [A.3] and [A.4] using only its velocity terms.

We note that [A.4] does not apply to, say, Brownian motion in which the 1st moment of the momentum flux (i.e. the left expression in [A.4] being the advective momentum flux) can be zero while the 2nd moment (i.e. the dispersive momentum flux) will not vanish. However, here and in what follows we consider the condition that the existence of an advective momentum flux (i.e. a nonzero α phase velocity) will dictate the occurrence of a dispersive momentum flux. Moreover, we conclude that the vanishing of $\overline{e_\alpha}^\alpha$ will also cause the disappearance of, $\overset{\circ}{e}_\alpha$, the deviation from the average. We thus assume that

[A.5.1] $\overset{\circ}{e}_\alpha = \Lambda_{e_\alpha}\overline{e_\alpha}^\alpha,$

in which Λ_{e_α} denotes the component of a, say empirical, factor that can be a scalar, a vector or a tensor of any rank. In view of [A.5.1] we write

$$\overline{\mathbf{d}_\alpha^M}^\alpha = \overline{\mathbf{A}_\alpha}^\alpha \overline{\rho_\alpha}^\alpha \overline{\mathbf{V}_\alpha^m}^\alpha, \quad \overline{\mathbf{A}_\alpha}^\alpha \equiv \overline{\Lambda_{\rho_\alpha}\Lambda_{V_\alpha^m}}^\alpha \tag{2.6}$$

and

$$\overline{(\rho_\alpha \mathbf{V}_\alpha^m)\overset{\circ}{\mathbf{V}}{}_\alpha^m}^\alpha = \overline{\mathbf{C}_\alpha}^\alpha \overline{\rho_\alpha}^\alpha \overline{\mathbf{V}_\alpha^m}^\alpha \overline{\mathbf{V}_\alpha^m}^\alpha, \quad \overline{\mathbf{C}_\alpha}^\alpha \equiv \overline{\mathbf{\Lambda}_{(\rho_\alpha V_\alpha^m)}\mathbf{\Lambda}_{V_\alpha^m}}^\alpha, \tag{2.7}$$

in which $\mathbf{\Lambda}_{(\rho_\alpha V_\alpha^m)}$ can be shown to be dependent on Λ_{ρ_α} and $\mathbf{\Lambda}_{V_\alpha^m}$.

By virtue of [A.5.1] and (2.6), we express [A.3] in the form:

[A.5.2] $1 \gg \|\overline{\mathbf{A}_\alpha}^\alpha\| \equiv \varepsilon$, suggesting that $\overline{\mathbf{A}_\alpha}^\alpha = \varepsilon \overline{\mathbf{B}_\alpha}^\alpha$ with $\|\overline{\mathbf{B}_\alpha}^\alpha\| = 1$,

and note that [A.5.1] together with (2.7), conforms [A.4] to read

[A.5.3] $1 \gg \|\overline{\mathbf{C}_\alpha}^\alpha\|$, which in view of [$A$.5.2], we assume that $\overline{\mathbf{C}_\alpha}^\alpha = \varepsilon \overline{\mathbf{D}_\alpha}^\alpha$.

By virtue of [A.5.2] and [A.5.3], we now rewrite (2.5) in the form:

$$\begin{aligned}
&\frac{\partial}{\partial t}\left(\theta_\alpha \overline{\rho_\alpha}^\alpha \overline{\mathbf{V}_\alpha^m}^\alpha\right) + \varepsilon \frac{\partial}{\partial t}\left(\theta_\alpha \overline{\mathbf{B}_\alpha}^\alpha \overline{\rho_\alpha^m}^\alpha \overline{\mathbf{V}_d^m}^\alpha\right) \\
&\quad = -\nabla \cdot \left[\theta_\alpha (\overline{\rho_\alpha}^\alpha \overline{\mathbf{V}_\alpha^m}^\alpha \overline{\mathbf{V}_\alpha^m}^\alpha - \overline{\boldsymbol{\sigma}_\alpha}^\alpha)\right] + \\
&\qquad + \theta_\alpha \overline{\rho_\alpha \mathbf{F}_\alpha}^\alpha - \varepsilon \nabla \cdot \left[\theta_\alpha \left(\overline{\mathbf{B}_\alpha}^\alpha + \overline{\mathbf{D}_\alpha}^\alpha\right) \overline{\rho_\alpha}^\alpha \overline{\mathbf{V}_\alpha^m}^\alpha \overline{\mathbf{V}_\alpha^m}^\alpha\right].
\end{aligned} \tag{2.8}$$

We note that as $\varepsilon \ll 1$, then an approximate solution to (2.8) can be obtained by decomposing it into a set of two coupled balance equations, each of a different order of magnitude. Moreover, since the solution of (2.8) depends on ε, we can expand its dependent variables $\big($e.g. $\overline{\rho_\alpha}^\alpha \approx \overline{\rho_{0\alpha}}^\alpha + \varepsilon \overline{\rho_{0\alpha}}^\alpha + \varepsilon^2 \overline{\rho_{2\alpha}}^\alpha + \cdots$; $\overline{\mathbf{V}_\alpha^m}^\alpha \approx \overline{\mathbf{V}_{0\alpha}^m}^\alpha + \varepsilon \overline{\mathbf{V}_{1\alpha}^m}^\alpha + \varepsilon^2 \overline{\mathbf{V}_{2\alpha}^m}^\alpha + \cdots\big)$ using terms associated with a polynomial of ε powers. An approximate solution to (2.8) can thus be obtained by solving an infinite set of momentum balance equations of descending order of magnitude. While the first (i.e. when ε = 0) balance equation is nonlinear and of the highest order of magnitude, the others are linear balance equations as they are combined with variables obtained from the solution of the equations that are of higher order magnitude. In view of (2.5) and (2.8), we can assume that the *dominant momentum balance equation*, reads

$$\frac{\partial}{\partial t}\left(\theta_\alpha \overline{\rho_\alpha}^\alpha \overline{\mathbf{V}_\alpha^m}^\alpha\right) = -\nabla \cdot \left[\theta_\alpha (\overline{\rho_\alpha}^\alpha \overline{\mathbf{V}_\alpha^m}^\alpha \overline{\mathbf{V}_\alpha^m}^\alpha - \overline{\boldsymbol{\sigma}_\alpha}^\alpha)\right] + \theta_\alpha \overline{\rho_\alpha \mathbf{F}_\alpha}^\alpha. \tag{2.9}$$

The validity of an assumption is justified by comparing the predictions of its resulting model with observations. As will be shown in the case of a fluid phase, under certain assumptions, (2.9) can conform to the well-known Darcy's linear momentum, to Forchheimer's law or to a momentum balance equation that governs the propagation of shock waves through porous media. The latter was verified, Levy *et al.* (1995), by shock tube experiments.

In view of (2.5) and (2.8) the balance equation assumed to be of a much lower order of magnitude, i.e., the *secondary momentum balance equation*, reads

$$\frac{\partial}{\partial t}\left(\theta_\alpha \overline{\mathbf{d}_\alpha^M}^\alpha\right) = -\nabla \cdot \left\{\theta_\alpha \left[\overline{\mathbf{d}_\alpha^M}^\alpha \overline{\mathbf{V}_\alpha^m}^\alpha + \overline{(\rho_\alpha \mathbf{V}_\alpha^m)\overset{\circ}{\mathbf{V}_\alpha^m}}^\alpha\right]\right\}. \tag{2.10}$$

Both, (2.9) and (2.10) are coupled via, $\overline{\mathbf{V}_\alpha^m}^\alpha$ the velocity of the α phase. In view of (2.6) and (2.7), we can rewrite (2.10) in the form:

$$\frac{\partial}{\partial t}\left(\theta_\alpha \overline{\mathbf{d}_\alpha^M}^\alpha\right) = -\nabla \cdot \left[\theta_\alpha (\mathbf{I} + \boldsymbol{\Omega}_\alpha) \overline{\mathbf{d}_\alpha^M}^\alpha \overline{\mathbf{V}_\alpha^m}^\alpha\right], \quad \boldsymbol{\Omega}_\alpha \equiv \overline{\mathbf{C}_\alpha}^\alpha \left(\overline{\mathbf{A}_\alpha}^\alpha\right)^{-1}, \tag{2.11}$$

which represents a wave equation propagating the $\overline{\mathbf{d}_\alpha^M}^\alpha$ quantity.

We note that although (2.9) and (2.11) are coupled, each is based on a different premise and thus can represent different characteristics. Based on the averaging procedure, the dominant macroscopic momentum balance equation (associated with the larger spatial scale), accounts also for transfer of microscopic flux of the phase extensive quantity through the microscopic interface of interacting phases. The macroscopic secondary momentum balance equation considers deviations from processes averaged in the considered *REV*. A valid possibility, when drag at the solid–fluid dominates, is that (2.9) can be approximated by Darcy's equation at the large spatial scale while, concurrently, (2.11) (or (2.10)) represents the governing of inertial flow at a smaller spatial scale. Moreover, we can solve (2.9) for $\overline{\mathbf{V}_\alpha^m}^\alpha$ and then estimate the magnitude of $\overline{\mathbf{d}_\alpha^M}^\alpha$ by solving (2.11).

2.2. THE MICROSCOPIC PRESSURE GRADIENT THROUGH THE SOLID–FLUID INTERFACE

In what follows we will further develop (2.9) in the form of NS equation accounting also for the microscopic pressure gradient transferred through the solid–fluid ($\mathcal{S}_{fS}$) interface.

Subtracting from (2.9) the product of $\overline{\mathbf{V}_\alpha^m}^\alpha$ with the mass balance equation for the α phase reads,

$$\theta\overline{\rho_\alpha}^\alpha \frac{\partial}{\partial t}\overline{\mathbf{V}_\alpha^m}^\alpha = -\theta_\alpha\overline{\rho_\alpha}^\alpha\overline{\mathbf{V}_\alpha^m}^\alpha\nabla\cdot\overline{\mathbf{V}_\alpha^m}^\alpha + \nabla\cdot(\theta_\alpha\overline{\sigma_\alpha}^\alpha) + \theta_\alpha\overline{\rho_\alpha\mathbf{F}_\alpha}^\alpha. \tag{2.12}$$

Let us consider the case of a saturated porous medium (i.e. $\alpha \equiv f-$fluid, and $\beta \equiv s-$solid) for which $\theta_f = \phi$, the porosity, and $\theta_s = 1-\phi$.

Referring to the fluid phase, let us assume that

[A.6] Newtonian fluid, and that
[A.7] only gravity body forces exist.

In view of [A.l] from which we obtain $\nabla\cdot(\theta_\alpha\overline{\sigma_\alpha}^\alpha) = \theta_\alpha\overline{\nabla\cdot\sigma_\alpha}^\alpha$, [$A$.6] and [$A$.7], we rewrite (2.12) in the form of the macroscopic NS equation which reads

$$\overline{\rho_{\mathrm{f}}}^f \frac{\mathrm{D}_{\overline{V_{fj}^m}^f}}{\mathrm{D}t}\left(\overline{V_{\mathrm{f}i}^m}^f\right) = \frac{\overline{\partial\tau_{\mathrm{f}ij}}^f}{\partial x_j} - \frac{\overline{\partial P}^f}{\partial x_i} - \overline{\rho_{\mathrm{f}} g\frac{\partial Z}{\partial x_i}}^f, \tag{2.13}$$

in which $\boldsymbol{\tau}_{\mathrm{f}}$ denotes the shear stress tensor of the Newtonian fluid and $g\partial Z/\partial x_i$ denotes the gravity acceleration in the Z direction.

In expanding $\partial P/\partial x_i$ of (2.13), in view of (2.2) and (2.3), we write

$$\phi\frac{\overline{\partial P}^f}{\partial x_i} \cong \phi\frac{\partial\overline{P}^f}{\partial x_j}T^*_{\mathrm{f}ji} + \frac{1}{\mathcal{U}_\circ}\int_{\mathcal{S}_{\mathrm{fS}}} \overset{\circ}{x}_i\frac{\partial P}{\partial x_j}\xi_{\mathrm{f}j}\,\mathrm{d}S. \tag{2.14}$$

The microscopic $\partial P/\partial x_j$ at the r.h.s. of (2.14) can be deduced from the microscopic NS equation at the $\mathcal{S}_{\mathrm{fS}}$ interface. In doing so, Levy *et al.* (1999) expanded the assumption made by Bear and Bachmat (1990) and assumed that

$$\left|\left(\rho_f\frac{\partial V_{\mathrm{f}j}^m}{\partial t} - \frac{\partial\tau_{\mathrm{f}ij}}{\partial x_i}\right)\xi_{\mathrm{f}j}\right| \ll \left|\left(\frac{\partial P}{\partial x_j} + \rho_{\mathrm{f}} g\frac{\partial Z}{\partial x_j} + \rho_{\mathrm{f}} V_{fi}^m\frac{\partial V_{\mathrm{f}j}^m}{\partial x_i}\right)\xi_{\mathrm{f}j}\right|.$$

Levy *et al.* (1999) specifically found approximations for, $V_{\mathrm{f}j}^m(\partial V_{\mathrm{f}i}^m/\partial x_j)$, the microscopic terms of the inertia transferred through the $\mathcal{S}_{\mathrm{fS}}$ interface. This yields the Forchheimer terms associated with the square velocity of the fluid, relative to the solid.

Instead, we will exchange $\partial P/\partial x_j$ with all flux terms of the microscopic *NS* equation. Thus, we will write

$$\int_{\mathcal{S}_{\mathrm{fS}}} \overset{\circ}{x}_i \frac{\partial P}{\partial x_j}\xi_{\mathrm{f}j}\ \mathrm{d}S = -\int_{\mathcal{S}_{f\mathrm{S}}} \overset{\circ}{x}_i \left[\rho_{\mathrm{f}}\left(\frac{\partial V^m_{\mathrm{f}j}}{\partial t} + V^m_{\mathrm{f}k}\frac{\partial V^m_{\mathrm{f}j}}{\partial x_k}\right) + \rho_{\mathrm{f}} g\frac{\partial Z}{\partial x_j} - \frac{\partial \tau_{\mathrm{f}kj}}{\partial x_k}\right]\xi_{\mathrm{f}j}\ \mathrm{d}S, \tag{2.15}$$

in which we add, in comparison with Levy *et al.* (1999), the approximations for, $\partial V^m_{fj}/\partial t$, the rate of the fluid velocity and, $\partial\tau_{\mathrm{f}kj}/\partial x_k$, the surface force due to shear.

The first term on the r.h.s. of (2.15), by virtue of the integral form of the mean value theorem, can be approximated to read

$$\begin{aligned}\frac{1}{\mathcal{U}_\circ}\int_{\mathcal{S}_{\mathrm{fS}}} \overset{\circ}{x}_i \rho_{\mathrm{f}} \frac{\partial V^m_{\mathrm{f}j}}{\partial t}\xi_{\mathrm{f}j}\ \mathrm{d}S &\cong \overline{\phi\rho_{\mathrm{f}}\frac{\partial V^m_{\mathrm{f}j}}{\partial t}}^{fs}\left(\frac{1}{\phi\mathcal{U}_\circ}\int_{\mathcal{S}_{\mathrm{fS}}} \overset{\circ}{x}_i\xi_{\mathrm{f}j}\ \mathrm{d}S\right)\\ &\cong \phi\overline{\rho_{\mathrm{f}}}^f\frac{\partial \overline{V^m_{\mathrm{f}j}}^f}{\partial t}\ (\delta_{ij} - T^*_{\mathrm{f}ij}),\end{aligned} \tag{2.16}$$

in which δ_{ij} denotes the components of the Kronecker delta function, $\overline{(\,)}^{fs}$ denotes an average over the $\mathcal{S}_{\mathrm{fS}}$ area. Note that in (2.16) and in what follows for any a and b variables, we use the approximations $\overline{a}^{fs} \cong \overline{a}^f$; $\overline{ab}^{fs} \cong \overline{a}^f\overline{b}^f$; $\overline{\partial a/\partial\zeta}^{fs} \cong \partial\overline{a}^f/\partial\zeta$, and $\partial/\partial\zeta$ denotes a derivative over time or space.

The fourth term on the r.h.s. of (2.15) expressed in its constitutive relation, reads

$$\int_{\mathcal{S}_{\mathrm{fS}}} \overset{\circ}{x}_i \frac{\partial \tau_{fkj}}{\partial x_k}\xi_{\mathrm{f}j}\ \mathrm{d}S = \int_{\mathcal{S}_{\mathrm{fS}}} \overset{\circ}{x}_i \left[\mu_{\mathrm{f}}\frac{\partial^2 V^m_{\mathrm{f}j}}{\partial x_k\partial x_k} + (\mu_{\mathrm{f}} + \lambda''_{\mathrm{f}})\frac{\partial}{\partial x_j}\left(\frac{\partial V^m_{\mathrm{f}k}}{\partial x_k}\right)\right]\xi_{\mathrm{f}j}\ \mathrm{d}S, \tag{2.17}$$

In which μ_{f} denotes the fluid dynamic viscosity and λ''_{f} denotes its second viscosity.

We add the assumption that

[A.8] no slip conditions prevail at, $\mathcal{S}_{\mathrm{fS}}$, the solid–fluid interface.

Thus the first term on the r.h.s. of (2.17) can be approximated to read

$$\begin{aligned}\frac{1}{\mathcal{U}_\circ}\int_{\mathcal{S}_{\mathrm{fS}}} \overset{\circ}{x}_i \mu_{\mathrm{f}} \frac{\partial^2 V^m_{\mathrm{f}j}}{\partial x_k\partial x_k}\xi_{\mathrm{f}j}\ \mathrm{d}S &\cong \overline{\phi\mu_{\mathrm{f}}\frac{\partial^2 V^m_{\mathrm{f}j}}{\partial x_k\partial x_k}}^{fs}\left(\frac{1}{\phi\mathcal{U}_\circ}\int_{\mathcal{S}_{\mathrm{fS}}} \overset{\circ}{x}_i\xi_{\mathrm{f}j}\ \mathrm{d}S\right)\\ &\cong \phi\overline{\mu_{\mathrm{f}}}^f\frac{\partial^2 \overline{V^m_{\mathrm{f}j}}^f}{\partial x_k\partial x_k}(\delta_{ij} - T^*_{\mathrm{f}ij}).\end{aligned} \tag{2.18}$$

The second term on the r.h.s. of (2.17) can be approximated by a first order difference, in the form

$$\frac{1}{\mathcal{U}_\circ}\int_{\mathcal{S}_{\mathrm{fs}}} \overset{\circ}{x}_i(\mu_{\mathrm{f}}+\lambda''_{\mathrm{f}})\frac{\partial}{\partial x_j}\left(\frac{\partial V^m_{\mathrm{f}k}}{\partial x_k}\right)\xi_{\mathrm{f}j}\ \mathrm{d}S$$

$$\cong \phi(\overline{\mu_{\mathrm{f}}}^f+\overline{\lambda''_{\mathrm{f}}}^f)\left[\frac{1}{\phi\mathcal{U}_\circ}\int_{\mathcal{S}_{\mathrm{fs}}}\overset{\circ}{x}_i\frac{(\partial V^m_{\mathrm{f}k}/\partial x_k)|_{\mathcal{S}_{\mathrm{fs}}}-(\partial V^m_{\mathrm{f}k}/\partial x_k)|_{\Delta}}{\Delta_C}\mathrm{d}S\right]$$

$$\cong -\frac{c_f}{\Delta^2_{\mathrm{f}}}\phi\left(\overline{\mu_{\mathrm{f}}}^f+\overline{\lambda''_{\mathrm{f}}}^f\right)\left(\overline{\partial V^m_{\mathrm{f}k}/\partial x_k}^f-\overline{\partial V^m_{\mathrm{s}k}/\partial x_k}^s\right)\frac{1}{\mathcal{S}_{\mathrm{fs}}}\int_{\mathcal{S}_{\mathrm{fs}}}\overset{\circ}{x}_i\ \mathrm{d}S, \tag{2.19}$$

where c_{f} denotes a shape factor, Δ_C denotes a characteristic, Δ, distance (aligned with $\xi_{\mathrm{f}j}$) from the $\mathcal{S}_{\mathrm{fs}}$ surface to the fluid within the pore space and $\Delta_{\mathrm{f}}(\equiv\phi\mathcal{U}_\circ/\mathcal{S}_{\mathrm{fs}}$, also related to $c_{\mathrm{f}}\Delta_C)$ denotes the hydraulic radius of the pore spaces.

Using the averaging rule for spatial derivative, we express the divergences of (2.19) in the form:

$$\phi\overline{\frac{\partial V^m_{\mathrm{f}k}}{\partial x_k}}^{\mathrm{f}}=\frac{\partial}{\partial x_k}\left(\phi\overline{V^m_{\mathrm{f}k}}^f\right)+\frac{1}{\mathcal{U}_\circ}\int_{\mathcal{S}_{\mathrm{fs}}}V^m_{\mathrm{f}k}\xi_{fk}\ \mathrm{d}S$$

$$\cong\frac{\partial}{\partial x_k}\left(\phi\overline{V^m_{\mathrm{f}k}}^f\right)+\overline{V^m_{\mathrm{S}k}}^{\mathrm{s}}\left(\frac{1}{\mathcal{U}_\circ}\int_{\mathcal{S}_{\mathrm{fs}}}\xi_{\mathrm{f}k}\ \mathrm{d}S\right)=\frac{\partial}{\partial x_k}\left(\phi\overline{V^m_{\mathrm{f}k}}^{\mathrm{f}}\right)-\overline{V^m_{\mathrm{s}k}}^{\mathrm{s}}\frac{\partial\phi}{\partial x_k}$$

$$=\frac{\partial q_{rk}}{\partial x_k}+\phi\frac{\partial\overline{V^m_{\mathrm{s}k}}^{\mathrm{s}}}{\partial x_k}, \tag{2.20}$$

in which $\mathbf{q}_r[\equiv\phi(\overline{\mathbf{V}^m_{\mathrm{f}}}^f-\overline{\mathbf{V}^m_{\mathrm{s}}}^{\mathrm{s}})=\phi\mathbf{V}_r]$ denotes the vector of the specific relative flux related to, $\mathbf{V}_{\mathrm{r}}$, the vector of the relative velocity, and

$$\overline{\frac{\partial V^m_{\mathrm{s}k}}{\partial x_k}}^{\mathrm{s}}=\frac{\partial\overline{V^m_{\mathrm{s}k}}^{\mathrm{s}}}{\partial x_k}+\frac{1}{(1-\phi)\mathcal{U}_\circ}\int_{\mathcal{S}_{\mathrm{fs}}}V^m_{sk}\xi_{sk}\ \mathrm{d}S$$

$$\cong\frac{\partial\overline{V^m_{sk}}^{\mathrm{s}}}{\partial x_k}+\frac{\overline{V^m_{sk}}^{\mathrm{s}}}{1-\phi}\left(\frac{1}{\mathcal{U}_\circ}\int_{\mathcal{S}_{\mathrm{fs}}}\xi_{sk}\ \mathrm{d}S\right)=\frac{\partial\overline{V^m_{sk}}^{\mathrm{s}}}{\partial x_k}+\frac{\overline{V^m_{sk}}^{\mathrm{s}}}{1-\phi}\frac{\partial\phi}{\partial x_k}. \tag{2.21}$$

In view of (2.18)–(2.21) we express (2.17) in the form:

$$\frac{1}{\mathcal{U}_\circ}\int_{\mathcal{S}_{\mathrm{fs}}} \overset{\circ}{x}_i \frac{\partial \tau_{\mathrm{f}kj}}{\partial x_k}\xi_{\mathrm{f}j}\ \mathrm{d}S \cong \overline{\mu_{\mathrm{f}}}^f \phi \frac{\partial^2 \overline{V_{\mathrm{f}j}^m}^f}{\partial x_k \partial x_k}(\delta_{ij} - T^*_{\mathrm{f}ij}) - \\ - \frac{c_f}{\Delta_{\mathrm{f}}^2}\left(\overline{\mu_{\mathrm{f}}}^f + \overline{\lambda_{\mathrm{f}}''}^f\right)\left(\frac{\partial q_{rk}}{\partial x_k} - \frac{\phi}{1-\phi}\overline{V_{sk}^m}^{\mathrm{s}}\frac{\partial \phi}{\partial x_k}\right)\Delta_{\overset{\circ}{x}i}, \tag{2.22}$$

where $\Delta_{\overset{\circ}{x}i}$ denotes the element of a vector (associated with $\overset{\circ}{x}_i$) representing the order of magnitude of the pore extent in the i-th coordinate direction, defined in the form:

$$\Delta_{\overset{\circ}{x}_i} \equiv \frac{1}{\mathcal{S}_{\mathrm{fS}}}\int_{\mathcal{S}_{\mathrm{fs}}} \overset{\circ}{x}_i\ \mathrm{d}S. \tag{2.23}$$

Hence, following Levy *et al.* (1999) and by virtue of (2.16) and (2.22), we rewrite (2.15) in the form

$$\frac{1}{\mathcal{U}_\circ}\int_{\mathcal{S}_{\mathrm{fs}}} \overset{\circ}{x}_i \frac{\partial P}{\partial x_j}\xi_{\mathrm{f}j}\ \mathrm{d}S \cong \frac{c_f}{2\Delta_{\mathrm{f}}^2}\phi\overline{\rho_{\mathrm{f}}}^f V_{rk}V_{rj}F_{kji} - g\overline{\rho_{\mathrm{f}}}^f(\delta_{i3} - T^*_{fi3}) + \\ + \left[\phi\overline{\mu_f}^f \frac{\partial^2 \overline{V_{\mathrm{f}j}^m}^f}{\partial x_k \partial x_k} + \phi\overline{\rho_{\mathrm{f}}}^f \frac{\partial \overline{V_{\mathrm{f}j}^m}^f}{\partial t} - \overline{\rho_{\mathrm{f}}}^f\overline{V_{sk}^m}^{\mathrm{s}}\left(\frac{\partial q_{rj}}{\partial x_k} + \phi\frac{\partial \overline{V_{sj}^m}^{\mathrm{s}}}{\partial x_k}\right)\right](\delta_{ij-T^*_{\mathrm{f}ij}}) - \\ - \frac{c_f}{\Delta_{\mathrm{f}}^2}\left(\overline{\mu_{\mathrm{f}}}^f + \overline{\lambda_{\mathrm{f}}''}^f\right)\left(\frac{\partial q_{rk}}{\partial x_k} - \frac{\phi}{1-\phi}\overline{V_{sk}^m}^{\mathrm{s}}\frac{\partial \phi}{\partial x_k}\right)\Delta_{\overset{\circ}{x}i} \tag{2.24}$$

in which $F_{kji}[\equiv (1/\mathcal{S}_{\mathrm{fS}})\int_{\mathcal{S}_{\mathrm{fs}}} \overset{\circ}{x}_i(\delta_{kj} - \xi_{fk}\xi_{fj})\mathrm{d}S]$ denotes the kji components of the Forchheimer tensor.

Actually, we note that (2.24) is the macroscopic approximation of (2.15) which expresses the exchange between the microscopic pressure gradient, at the solid–fluid interface, with the microscopic NS equation. In view of Levy *et al.* (1999) we note that (2.24) addresses the extensions to Forchheimer terms emerging from the microscopic terms of the fluid velocity rate and the surface force due to shear.

In the followings we will refer to the macroscopic quantities of the fluid phase and its velocity will be regarded as being mass weighted. Thus, e.g., symbols as in $\overline{(\ )_{\mathrm{f}}^m}^f$, will be omitted.

2.3. MACROSCOPIC FORMS OF THE NAVIER–STOKES EQUATION

Following Bear and Bachmat (1990) and by virtue of (2.24), we rewrite (2.13) as the extended macroscopic NS equation

$$\begin{aligned}
&\phi\rho\left[\frac{\mathrm{D}_{V_j}}{\mathrm{D}t}(V_i)+\frac{\partial V_j}{\partial t}(\delta_{ij}-T^*_{ij})\right]\cong-\phi\left(\frac{\partial P}{\partial x_j}+\rho g\frac{\partial Z}{\partial x_j}\right)T^*_{ij}-\\
&-\frac{c_f}{2\Delta_f^2}\phi\rho V_{rk}V_{rj}F_{kji}-\left[\phi\mu\frac{\partial^2 V_j}{\partial x_k\partial x_k}-\rho V_{sk}\left(\frac{\partial q_{rj}}{\partial x_k}+\phi\frac{\partial V_{sj}}{\partial x_k}\right)\right](\delta_{ij}-T^*_{ij})+\\
&+\mu\left[\frac{\partial}{\partial x_j}\left(\frac{\partial q_{ri}}{\partial x_j}+\phi\frac{\partial V_{si}}{\partial x_j}\right)-\frac{c_f}{\Delta_{\mathrm{f}}^2}\alpha_{ij}q_{rj}\right]+(\mu+\lambda'')\left[\frac{\partial}{\partial x_i}\left(\frac{\partial q_{rj}}{\partial x_j}+\phi\frac{\partial V_{sj}}{\partial x_j}\right)-\right.\\
&\left.-\frac{\partial V_j}{\partial x_j}\frac{\partial\phi}{\partial x_i}+\frac{c_{\mathrm{f}}}{\Delta_{\mathrm{f}}^2}\left(\frac{\partial q_{rj}}{\partial x_j}-\frac{\phi}{1-\phi}V_{sj}\frac{\partial\phi}{\partial x_j}\right)\Delta_{\overset{\circ}{x}i}\right],
\end{aligned} \tag{2.25}$$

where $\alpha_{ij}[\equiv(1/\mathcal{S}_{\mathrm{fS}})\int_{\mathcal{S}_{\mathrm{fS}}}(\delta_{ij}-\xi_i\xi_j)\mathrm{d}S]$ denotes the ij components of a cosine directions tensor.

Let us now assume that

[A.9] The flow is *isochoric* at the microscopic level [i.e. $(\partial V_j/\partial x_j)(\partial\phi/\partial x_i)=0$].

[A.10] The velocity of the solid phase is negligible in comparison to the fluid velocity (i.e. $\|\mathbf{V}\|\gg\|\mathbf{V}_\mathrm{s}\|$).

Actually by virtue of [A.10] we conclude that

$$\mathbf{q}_r\cong\mathbf{q}=\phi\mathbf{V},\quad\left|\frac{\partial q_i}{\partial x_j}\right|\gg\left|\phi\frac{\partial V_{si}}{\partial x_j}\right|,\quad\left|\rho V_{sk}\frac{\partial q_j}{\partial x_k}\right|\ll\left|\phi\mu\frac{\partial^2 V_j}{\partial x_k\partial x_k}\right|,$$
$$\left|\frac{\partial q_j}{\partial x_j}\right|\gg\left|\frac{\phi}{1-\phi}V_{sj}\frac{\partial\phi}{\partial x_j}\right|.$$

[A.11] The fluid velocity rate summed over the microscopic solid–fluid interface is negligible in comparison to the fluid velocity rate averaged over the volume of the REV scale.

[A.12] The friction at the solid–fluid interface is dominant in comparison to the friction between the fluid layers $\left[\text{i.e.}\left|\frac{c_\mathrm{f}}{\Delta_\mathrm{f}^2}\alpha_{ij}q_j\right|\gg\left|\frac{\partial}{\partial x_j}\left(\frac{\partial q_i}{\partial x_j}\right)\right|\right]$ as well as to the friction resulting from the microscopic shear at that interface $\left[\text{i.e.}\left|\phi(\delta_{ij}-T^*_{ij})\frac{\partial^2 V_j}{\partial x_k\partial x_k}\right|\ll\left|\frac{c_\mathrm{f}}{\Delta_\mathrm{f}^2}\alpha_{ij}q_j\right|\gg\left|\frac{c_\mathrm{f}}{\Delta_\mathrm{f}^2}\frac{\partial q_{rj}}{\partial x_j}\Delta_{\overset{\circ}{x}i}\right|\right]$.

By virtue of [A.9]–[A.12] we rewrite, (2.25), the NS equation in the form:

$$\phi\rho\frac{\mathrm{D}_{V_j}}{\mathrm{D}t}(V_i)\cong -\phi\left(\frac{\partial P}{\partial x_j}+\rho g\frac{\partial Z}{\partial x_j}\right)T^*_{ij}-\frac{c_{\mathrm{f}}}{2\Delta_{\mathrm{f}}^2}\phi\rho V_k V_j F_{kji}-\mu\frac{c_{\mathrm{f}}}{\Delta_{\mathrm{f}}^2}\alpha_{ij}q_j. \tag{2.26}$$

Further, let us assume that

[A.13] The flow is fully developed $\left[\text{i.e. } \phi\rho\frac{\mathrm{D}_{V_j}}{\mathrm{D}_t}(V_i)\ll\mu\frac{c_{\mathrm{f}}}{\Delta_{\mathrm{f}}^2}\alpha_{ij}q_j\right]$.

In view of [A.13] we note that (2.26) conforms to *Forchheimer Law* which reads

$$q_i+\frac{\rho/\mu}{2\phi}\alpha_{ij}^{-1}F_{kji}q_k q_j=-\frac{k_{ij}}{\mu}\left(\frac{\partial P}{\partial x_j}+\rho g\frac{\partial Z}{\partial x_j}\right), \tag{2.27}$$

where k_{ij} is regarded as the intrinsic permeability tensor expressed by

$$k_{ij}\equiv k_{\mathrm{c}}\alpha_{ij}^{-1}T^*_{ij}, \tag{2.28}$$

and k_{c} denotes the characteristic permeability

$$k_{\mathrm{c}}=\frac{\phi_{\mathrm{c}}\Delta_{\mathrm{f}}^2}{c_{\mathrm{f}}}, \tag{2.29}$$

related to, ϕ_{c}, the characteristic porosity.[†]

Let us express quantities as products of their, $(\ )_c$, characteristic values with their, $(\ )^*$, nondimensional ones that are of unit orders [i.e. $(\ )=(\ )_c(\ )^*$], e.g., $F_{kji}=\mathring{x}_c(F_{kji})^*$ in which $\mathring{x}_i=\mathring{x}_c(\mathring{x}_i)^*$.

Assuming that

[A.14] $\quad c_{\mathrm{f}}\mathring{x}_{\mathrm{c}}\cong\Delta_{\mathrm{f}}$,

we obtain by virtue of (2.29) and [A.14]

$$\mathring{x}_{\mathrm{c}}\cong\sqrt{\frac{k_{\mathrm{c}}}{\phi_{\mathrm{c}}c_{\mathrm{f}}}}. \tag{2.30}$$

We note that $\mathring{x}_{\mathrm{c}}$ actually represents a characteristic length of the porous medium. Rewriting the l.h.s. of (2.27) in its nondimensional form, $\left[\text{i.e. } (\phi_{\mathrm{c}}V_{\mathrm{c}})(q_i)^*+[(\rho_{\mathrm{c}}/\mu_{\mathrm{c}})\mathring{x}_{\mathrm{c}}\phi_{\mathrm{c}}V_{\mathrm{c}}^2]\left(\frac{\rho/\mu}{2\phi}\alpha_{ij}^{-1}F_{kji}q_k q_j\right)^*\right]$ and assuming that

[†]Note that for a one-dimensional case, say when neglecting gravitation, (2.27) is written in the form of $q+a|q|q=-(k/\mu)(\partial P/\partial x)$.

[A.15] $1 \gg \left| V_c \sqrt{k_c/(\phi_c c_f)}/(\mu_c/\rho_c) \right| \equiv Re$ (i.e. Reynolds number for a porous medium),

then in view of [A.15], we note that (2.27) conforms to a linear momentum balance equation similar to *Darcy's Law* (i.e. for $\rho = \text{const}$) namely,

$$q_i \cong -\frac{k_{ij}}{\mu}\left(\frac{\partial P}{\partial x_j} + \rho g \frac{\partial Z}{\partial x_j}\right). \tag{2.31}$$

3. Shock Waves through a Highly Deformable Porous Medium

Extending the theory developed by Sorek *et al.* (1992), the macroscopic theoretical basis for nonlinear wave motion in multiphase deformable porous media was introduced by Levy *et al.* (1995). In Levy *et al.* (1995), the fluid momentum balance equation is similar to the form of (2.26). Using a dimensional analysis it was shown that during the wave period (following an abrupt change in fluid's pressure and temperature) the momentum flux accounting for the drag in (2.26), is negligible. Numerical simulations with the one-dimensional version of this model (Levy *et al.*, 1996) proved to yield excellent agreement with experimental observations, concerning almost nondeformable porous materials. The results of the experimental study of Levy *et al.* (1993) with 40 mm long sample made of SiC having 10 pores per inch and an incident-shock-wave Mach number of 1.378, for the pressure histories of air at various locations along the shock tube, are presented in Figure 1. In Levi-Hevroni *et al.* (2002), following Levy *et al.* (1995), we consider a solid matrix that is capable to undergo extremely large deformations. Consequently, the constitutive law was expressed in terms of, $\dot{\boldsymbol{\sigma}}$, the tensor of incremental stress rate being a function of, $\dot{\boldsymbol{\varepsilon}}$, the incremental strain rate tensor, i.e., $\dot{\boldsymbol{\sigma}} = f(\dot{\boldsymbol{\varepsilon}})$. Actually, this follows the constitutive law of stress being a function of strain $\boldsymbol{\sigma} = f(\boldsymbol{\varepsilon})$, which can be valid for static loadings. Such a change resulted in an additional differential equation, which required an additional integration. Furthermore, the interface between the solid and the gaseous phases had to be tracked. As a consequence, in Levi-Hevroni *et al.* (2002) a mixed Lagrangian and Eulerian method was adopted when simulating tracking of the solid matrix moving front. Hence, the mass and momentum balance equations of the solid matrix were expressed in Lagrangian coordinates along a particle pathline.

To verify the performance of this approach, simulations were compared against the shock tube experiments of Levy *et al.* (1993) and the one-dimensional simulations (Levy *et al.*, 1996) of a porous matrix undergoing small deformations. The gas pressure histories upstream of the porous material, on the side-wall inside the porous material and at the end-wall are

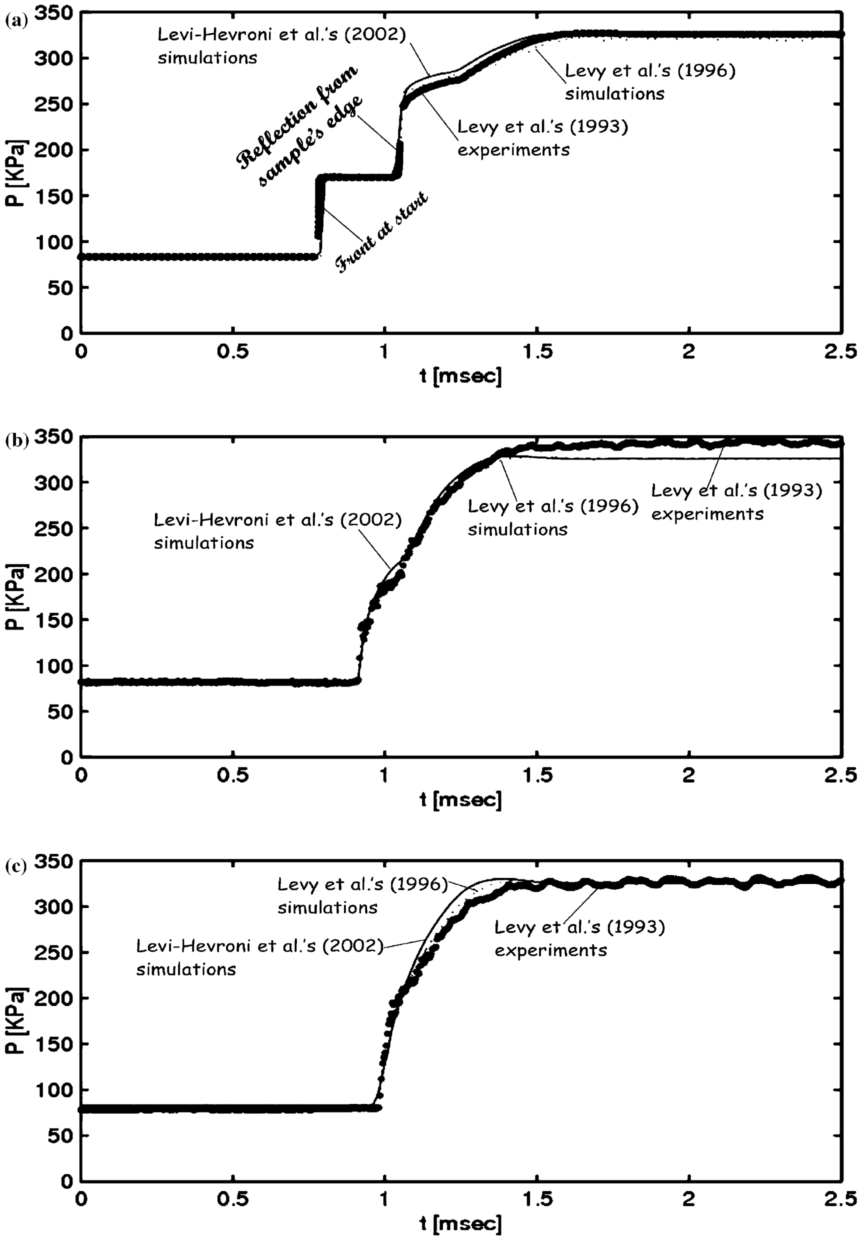

Figure 1. Experimental results and numerical predictions [dotted line - Levy *et al.* (1996) and solid line - Levi-Hevroni *et al.* (2002)] of the gas pressure histories (after Levi-Hevroni *et al.* (2002)) using a 40 mm long silicon carbide sample with 10 pores per inch and average porosity of 0.728 ± 0.016. Incident-shock wave Mach number in this experiment was $M_s = 1.378$. (a) Upstream 43 mm ahead the porous material front edge. (b) Along the shock tube side-wall inside the porous material. 23 mm from end-wall. (c) At the shock tube end-wall.

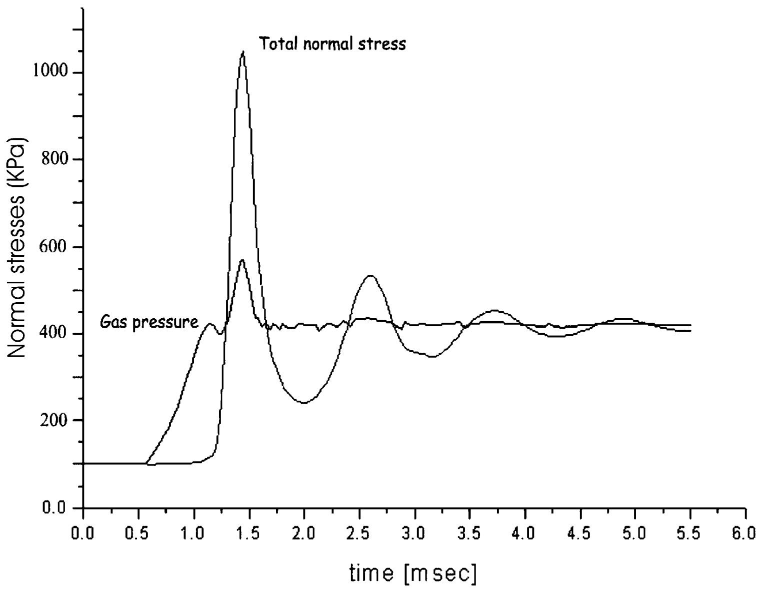

Figure 2. Simulated gas pressure and effective stress histories at the shock tube end-wall (after Levi-Hevroni *et al.* (2002)). The line labeled as *gas pressure* indicates the gas wave within the sample pores. The line labeled as *total normal stress* indicates the wave propagating through the sold part of the porous sample. The total-normal-stress shows the overall pressure exerted on the end-wall, indicating that the porous sample causes a pressure increase from about 410 KPa to about 1050 KPa. Numerical results of Levi-Hevroni *et al.* (2002) are in excellent, consistent, agreement with the foam experiments of Skews *et al.* (1993).

shown in Figure 1(a)–(c), respectively. Comparisons clearly indicate that the developed numerical code in Levi-Hevroni *et al.* (2002) reproduced the test problem very well.

We are not aware of experimental data concerning highly deformable porous medium. Hence, to fully validate the theoretical model and its numerical simulations as developed in Levi-Hevroni *et al.* (2002), only qualitative comparisons and physical behavior were examined. Figure 2 illustrates the calculated gas pressure and effective stress histories at the end-wall. It is clearly evident that two waves arrive at the end wall. The one moving in the gas, faster than the one moving in the solid matrix, is in excellent consistent agreement with the foam experiments of Skews *et al.* (1993). We note from Figure 2 that the peak effective stress (total pressure) is clearly reproduced by the simulation in Levi-Hevroni *et al.* (2002), which also resulted in a pressure amplification of about 12 similar to that reported by Skews *et al.* (1993).

The simulated trajectory of the front edge of the flexible porous material and the density field of the solid matrix are depicted in Figure 3. We also note that the front surface of the foam, first undergoes about 80%

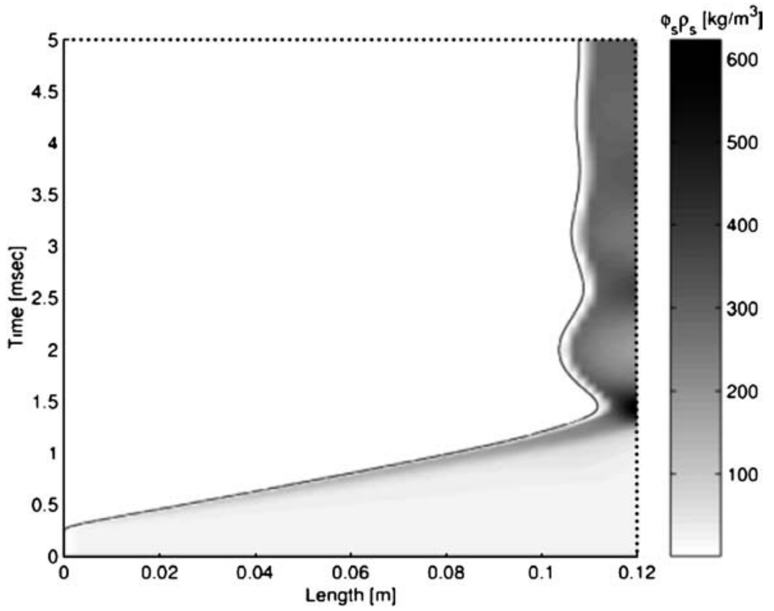

Figure 3. Evolution of the sample solid phase spatial density field and the trajectory of its front edge, as simulated by Levi-Hevroni *et al.* (2002). The undulate trajectory that decays in time follows the gas pressure inside the sample that is due to the periodic structure of alternating rarefaction and compression waves propagating back and forth between the front and back edges. The highest pressure is obtained behind the shock wave reflecting from the end-wall. Coupling between the motion of the sample/gas interface and the inside striking wave (shock/compression that increases the gas pressure and induces a velocity in the propagation direction) or rarefaction (i.e. decreases gas pressure and causes an opposite velocity) is clearly evident. Simulation results are similar to experimental observations by Skews *et al.* (1993).

deformation before it started to retreat backwards. In addition the foam wave head, which was reported by Skews *et al.* (1993), can clearly be seen in the foam domain.

The contact surface of the gas which originally filled the pores and was pushed out, was found experimentally by Skews *et al.* (1993) and reported in Levi-Hevroni *et al.* (2002) to be reproduced numerically. The calculated gas density field and the trajectory of the foam front edge are depicted in Figure 4.

From the experimental studies of Gvozdeva *et al.* (1985), we note that, to some extent, the peak in the solid effective stress (total pressure) depends on the lengths of the foam slab. The longer the foam slab the higher is the peak of the effective stress. This phenomenon was also reproduced by simulation, Levi-Hevroni *et al.* (2002), as depicted in Figure 5

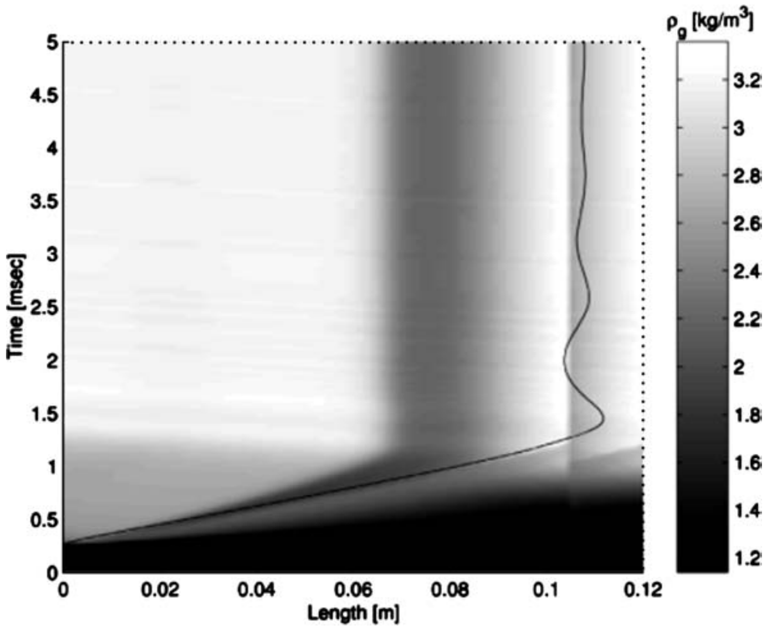

Figure 4. Calculated gas density field and front edge trajectory of the flexible elasto-plastic porous sample (after Levi-Hevroni *et al.* (2002)). We note the contact surface due to gas emerging from the sample porous matrix, after it had reached its utmost deformation. This very large deformation depleted the sample pores and forced the gas to flow across the sample/gas interface. Simulation results are similar to the experimental observations of Skews *et al.* (1993).

where the pressure histories at the end wall for three flexible foam slabs having the lengths 60, 90 and 120 mm are shown. As can be seen the pressure amplifications corresponding to these three cases are about 6, 8.25 and 10.5, respectively. It is also interesting to note that regardless of the length of the foam slabs, the waves at the end-wall approach after a few milliseconds with the same pressure.

4. Summary

Rigorous averaging, on the basis of the *REV* concept, of the microscopic *NS* equation produced two coupled macroscopic momentum equations each addresses its own spatial scale. Although the one associated with the smaller spatial scale is habitually assumed to be less dominant, it is however suggested that it can not be negligible in cases of significant deviation from the average fluid velocities and/or for heterogeneity in fluid properties. Moreover, it presents a feasible possibility of coupled formulation between a dominant Darcy law and a secondary macroscopic balance equation accounting for inertial effects at a smaller spatial scale.

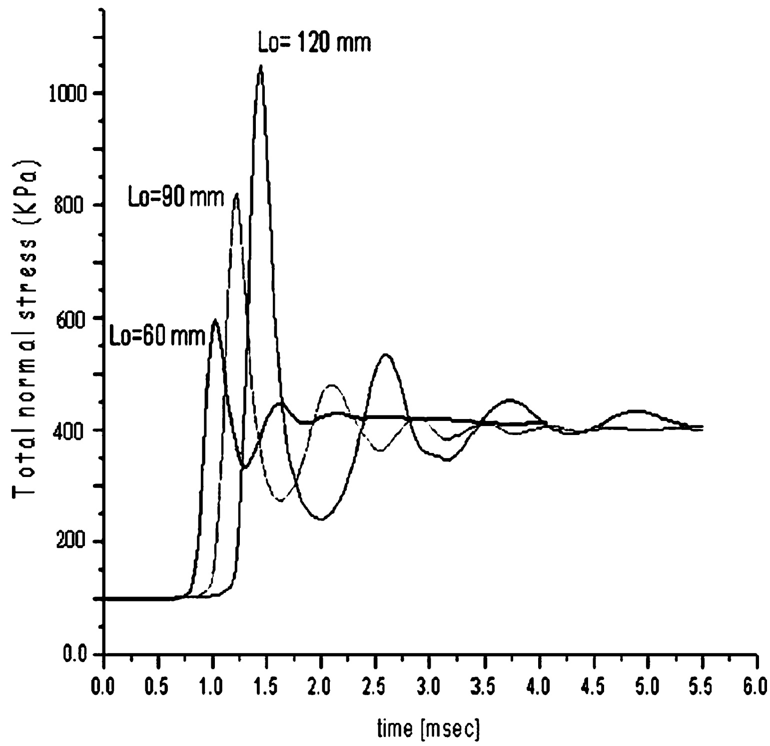

Figure 5. Pressure histories at the shock tube end-wall for different lengths of flexible foam slabs (after Levi-Hevroni *et al.* (2002)). We note that the peak pressure increases as the sample length increases while the shape of the pressure pulse at the end-wall remains similar. Simulations are consistent with the experiment results provided by Gvozdeva *et al.* (1985).

Focusing on the dominant macroscopic momentum balance equation, we had summed up the transfer of the pressure gradient at the microscopic solid–fluid interface of a saturated matrix, and obtained the full extent of Forchheimer terms accounting for the square of the relative velocity as well as its temporal rate. This led to an extension of the macroscopic *NS* equation which depending on the dominance of its terms can be approximated to a nonlinear wave equation, to the form of Forchheimer law or to Darcy's law.

As one specific outcome accounting for Forchheimer terms, we present the modeling of shock wave propagating through a rigid porous matrix (Levy *et al.*, 1995) and an extremely deformable one (Levi-Hevroni *et al.*, 2002). Results of the simulations are in very good quantitative and qualitative agreement with data of available experiments. These authors rely on (2.26) without drag (last term on the r.h.s) at the solid–fluid interface, we thus consider their simulations as examples validating the current developments.

References

Auriat, J. L., Strzelecki, T., Bauer, J. and He, S.: 1990, Porous deformable media saturated by a very compressible fluid: quasi-statics, *Eur. J. Mech. A/Solids*, **9**(4), 373–392.

Bear, J. and Bachmat, Y.: 1990, *Introduction to Modeling of Transport Phenomena in Porous Media*, *Kluwer Academic Publishers*, Dordrecht, The Netherlands.

Bear, J. and Sorek, S.: 1990, Evolution of governing mass and momentum balance equations following an abrupt pressure impact in a porous medium, *Transport in Porous Media* **5**, 169–185.

Bear, J., Sorek, S., Ben-Dor, G. and Mazor, G.: 1992, Displacement waves in saturated thermoelastic porous media. I. Basic equations, *Fluid Dynamic Res* **9**, 155–164.

Biot, M. A.: 1956, Theory of propagation of elastic waves in a fluid-saturated porous solid. I. Low frequency range, *J. Acoust. Soc. Am.* **28**, 2, 168–178.

Gvozdeva, L. G., Faresov, Yum, Fokeev, V. P.: 1985, Interaction between air shock waves and porous compressible materials, *Sov. Phys. Appl. Math. and Tech. Phys.* **3**, 111.

Levy, A., Ben-Dor, G., Skwes, S. and Sorek, S.: 1993, Head-on collision of normal shock waves with rigid porous materials, *Exp. Fluids* **15**, 183.

Levy, A., Sorek, S., Ben-Dor, G. and Bear, J.: 1995, Evolution of the balance equations in saturated thermoelastic porous media following abrupt simultaneous changes in pressure and temperature, *Transport in Porous Media*, **21**, 241–268.

Levy, A., Ben-Dor, G. and Sorek, S.: 1996, Numerical investigation of the propagation of shockwaves in rigid porous materials: development of the computer code and comparison with experimental results, *J. Fluid Mech.* **324**, 163.

Levy, A., Levi-Hevroni, D., Sorek, S. and Ben-Dor, G.: 1999, Derivation of Forchheimer terms and their verification by application to waves propagation in porous media, *Int. J. MultiPhase Flow* **25**, 683–704.

Levi-Hevroni, D., Levy, A., Ben-Dor, G. and Sorek, S. 2002, Numerical investigation of the propagation of planar shock waves in saturated flexible porous materials: development of the computer code and comparison with experimental results, *J. Fluid Mech.* **462**, 285–306.

Nikolaevskiy, V. N. Basniev, K. S., Gorbunov, A. T. and Zotov, G. A.: 1970, *Mechanics of Porous Saturated Media*, Nedra, Moscow (in Russian).

Nikolaevskiy, V. N.: 1990, *Mechanics of Porous and Fractured Media*, World Scientific, Singapore.

Nikolaevskiy, V. N.: 1996, *Geomechanics and Fluidodynamics*, Kluwer Academic Publishers, Dordrecht.

Skews, B. W., Atkins, M. D. and Seitz, M. W.: 1993, The impact of shock wave on porous compressible foams, *J. Fluid Mech.* **253**, 245.

Sorek, S., Bear, J., Ben-Dor, G. and Mazor, G.: 1992, Shock waves in saturated thermoelastic porous media, *Transport Porous Media* **9**, 3–13.

Sorek, S., Levy, A., Ben-Dor, G. and Smeulders, D.: 1999, Contributions to theoretical/experimental developments in shock waves propagation in porous media, *Transport in Porous Media* **34**(1/3), 63–100.